Trans. JWRI, Vol. 30,(2001), No. 1

Microjoining Process in Electronic Packaging and Its Numerical Analysis †

Yasuo TAKAHASHI* and Tie GANG **

Abstract

The present study was carried out for the purpose of understanding interfacial deformation processes during solid state inner lead bonding, which is used in electronic packaging. At first, the representative microjoining processes are summarized by showing some photos and illustrations. After that, the interfacial deformation between the electric pad and the inner lead is analyzed, using numerical simulations. In particular, two effects of the bump thickness and the mechanical property on the interfacial extension are analyzed. The numerical simulations are carried out by using a finite element method (FEM), which can be applied for large deformation of rate sensitivity materials.

KEY WORDS: (TAB) (Inner lead bonding)(Middle lead bonding) (Numerical simulation) (Bump) (Interconnection) (Interfacial deformation) (Bonding temperature) (Pad) (Fine lead)

1. Introduction

Electronic packaging generally consists of the interconnection (microjoining) within an IC package and the assembly of various chips, components and LSI or IC packages onto the print circuit board (PCB). The latter is manufactured by various microsoldering processes such as reflow soldering, vapor phase soldering and so on. The minimum size level of the solder joints on the PCB being less than a few hundred μm. On the other hand, the size of microjoining processes within the IC package is now form 30μm to 80 μm as a pitch distance. The dimension will decrease more and more, because of necessity of high density interconnection. In the present review, the trend of the microjoining process within the IC package is summarized and its numerical simulation is described.

2. Microjoining process used in electronic packaging

Microjoining processes used for the interconnection between IC chips and the lead frame (electric circuit) within the IC package are usually classified into three kinds of microjoining processes, i.e., wire bonding (WB), tape automatic bonding (TAB or tape carrier packaging), and flip chip attachment as illustrated in Fig. 1.

The wire bonding is now a very popular process because of its flexibility to changes in the electric circuit design. It is not too much to say that the wire bonding is the most frequently used among all welding processes used today. The minimum diameter of wire is 10 μm and the pitch distance is 40 μm [1, 2].

TAB, which is illustrated in Fig. 2, is also very often used for the inner lead bonding for LCD (liquid crystal display) and ASIC (custom IC) (see in Fig. 3). TAB is usually carried out by a gang bonding. The pitch distance and the width of leads in TAB inner lead bonding are, respectively, being 40 μm and 10 μm as shown in Fig. 4.

Recently, the flip chip bonding as shown in Fig. 5 is very actively being researched because of the necessity of high density packaging and chip size packaging (CSP). Flip chip bonding is usually carried out by solid (Au) balls, solder balls, or sometimes anisotropic conductive adhesive with micro capsule Ag filler [3]. The range of ball diameters is usually from 200 to 300 μm, regardless of the kinds of ball-material. Flip chip bonding by solder balls can be said to be the finest microsoldering. the thermal stress during using the flip chip bonded IC becomes a serious problem

† Received on August 1st, 2001

* Assosiate Professor JWRI, Osaka University

** Visiting Researcher, JWRI, Osaka University, Professor of Harbin Institute of Technology, National Key Laboratory of Advanced Welding Production Technology

Transactions of JWRI is published by Joining and Welding Research Institute of Osaka University, Ibaraki, Osaka 567-0047, Japan.

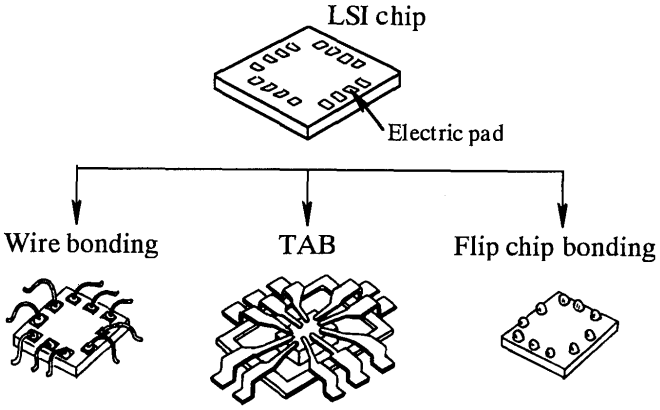

Fig. 1 Microjoining for interconnection within IC package.

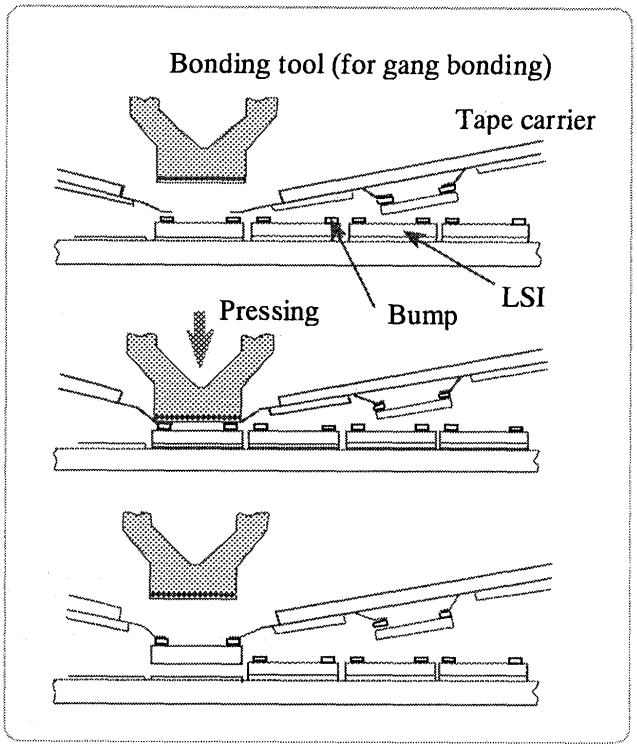

Fig. 2 Schematic illustration of TAB process.

for relaibility, because the flip chip attachment is a very compact interconnection without any lead. On the other hand, in WB and TAB, wires and leads used can be useful to relax the thermal strain.

In the present paper, the inner lead bonding in TAB process is mainly discussed, based on the numerical results. The purpose of the present study is to understand the mechanism of the solid state microjoining process and the interfacial extension which produces metallic bonds.

One of the authors has carried out the numerical studies for solid state welding and joining processes [4-6], and

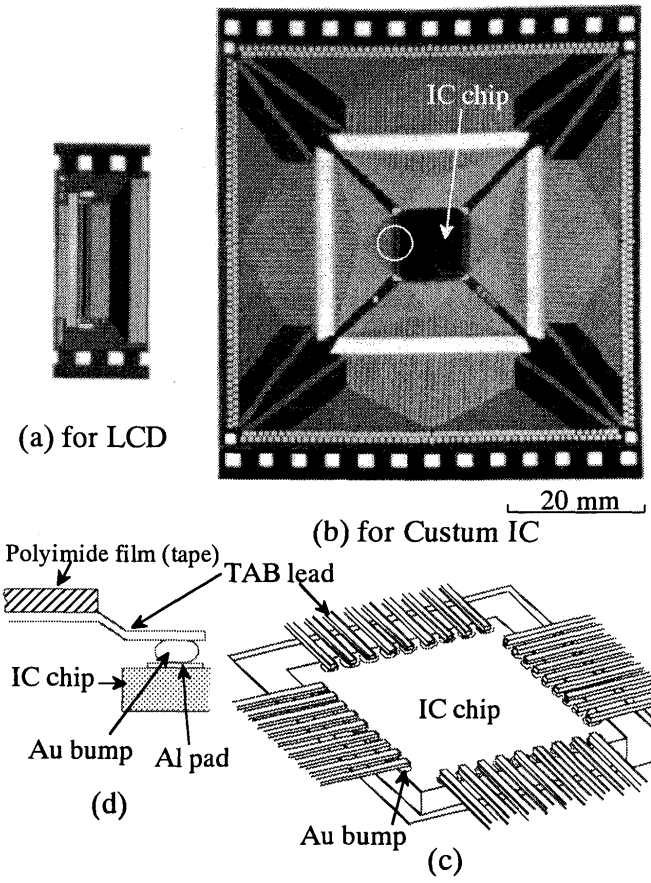

Fig. 3 Photos of TAB film and schematic illustration of interconnection by TAB process. (a) for LCD, (b) for ASIC, (c) illustration of inner lead bonds,and (d) illustration of cross section of TAB lead, Au bump, Al pad and IC chip. The white circle in (b) denotes the position of inner lead bonding.

analyzed the mechanism of interfacial extension along the bond-interface, because the interfacial extension breaks the oxide film on the bonding surface into small pieces when creating the metallic bond [7]. The interfacial extension is closely related with thesurface exposure ψ, which is an important parameter for representing the degree of bonding between metal surfaces, and is given by

$$\psi = (1 - G_d) \cdot \frac{\varepsilon_i}{1 + \varepsilon_i} , \qquad (1)$$

where G_d is the ductility of surface contamination or oxide film, and ε_i is the interface extension (strain). Therefore, knowledge of the local interfacial extension during solid state microjoining is very important in researching the bonding mechanism. Furthermore, the computer simulation makes it possible to visualize the lead deformation and makes it easy to understand the bonding process.

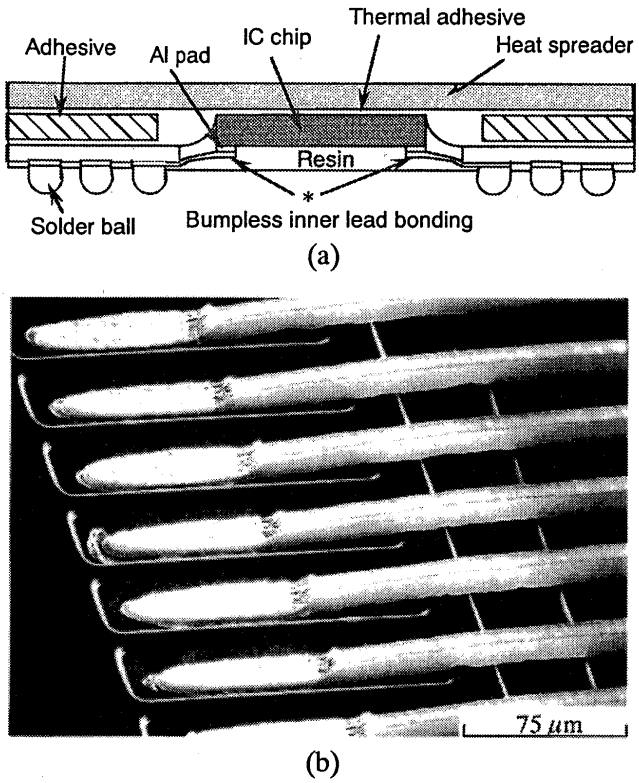

Fig. 4 Example of TAB bumpless bonding. (a) Tape ball grid array (TBGA) package and (b) photo of bumpless inner lead connections, the position of which is denoted in (a) by mark * 2).

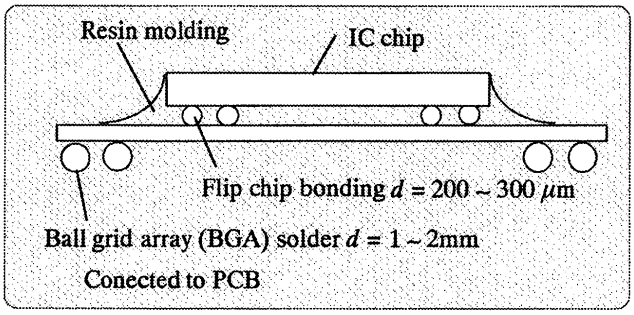

Fig. 5 Schematic illustration of flip chip bonding within BGA package.

3. Pull Strength of TAB in Experimental Results

Fig. 6 shows scanning electron microphotographs after TAB inner lead bonding (gang bonding), in which (a) is for the solid state bonding of gold plated copper lead to gold bump on aluminium pad and (b) for the liquid phase bonding of tin plated copper lead to gold bump on aluminium pad. In (b), Sn and Au eutectic structure is produced around the bonded zone and the fillet and the mark made by melting is observed at the both sides of TAB leads.

Fig. 7 shows the pull strength of TAB inner lead bonding under the condition of the tool head temperature T_t =

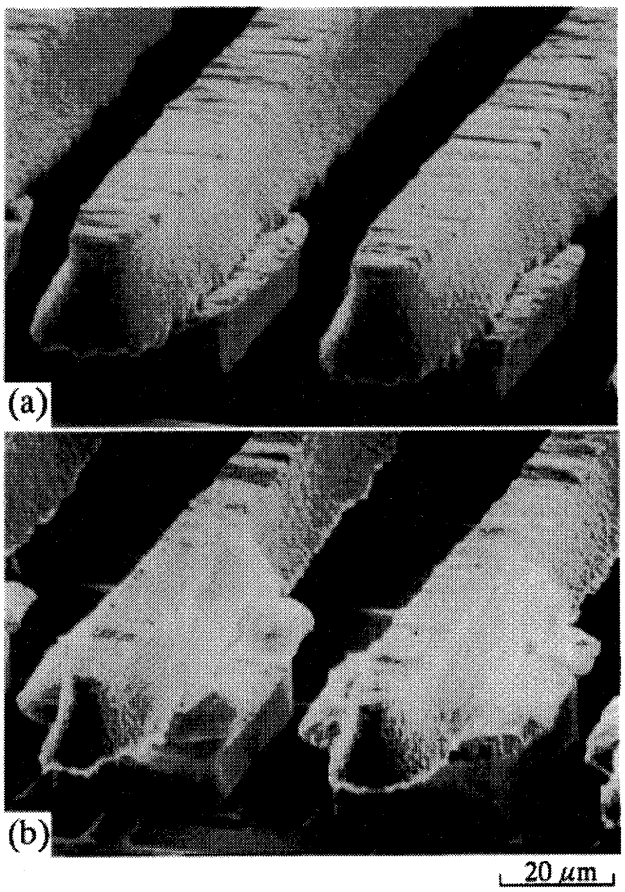

Fig. 6 TAB inner lead bonding (gang bonding without ultrasonic vibration). Straight bumps are formed on pads before bonding. Tool head temperature T_t = 773 K. (a) Au/Au bonding, W = 20gf/lead (P = 258 MPa). t = 1.0 s, and (b) Sn plated lead/Au bump bonding, W = 10 gf /lead (P = 129 MPa) and t = 0.1 s.

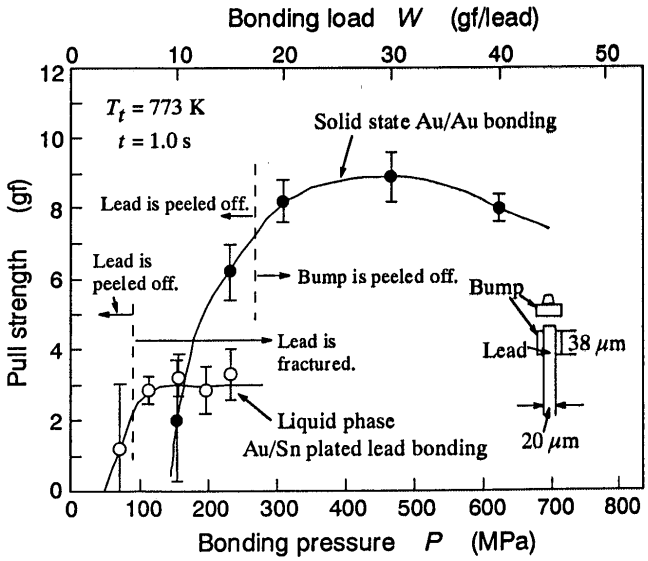

Fig. 7 Pull strength of TAB inner lead bonding which has been shown in Fig. 6, depending on bonding pressure.

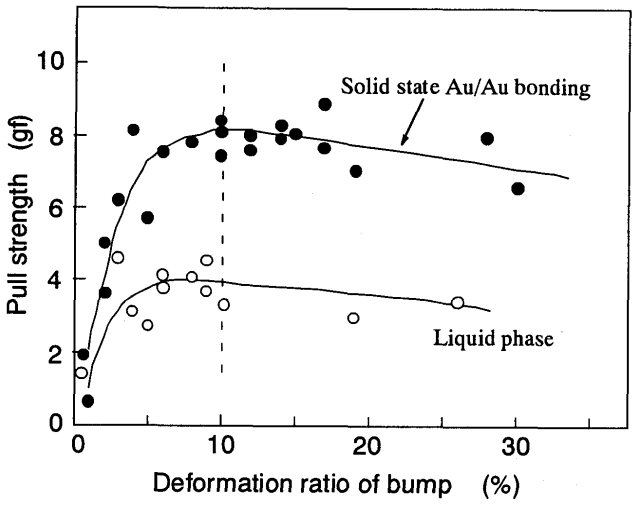

Fig. 8 Pul strength of TAB inner lead bonding with bump, depending on deformation ratio. (T_t = 773 K)

773 K and the bonding time t = 1.0 s, together with the illustration about sizes of lead and bump used in the bonding tests. As seen in Fig. 7, the pull strength of the Au/Au bonding under the solid state condition is much larger than that of liquid phase (Sn/Au) bonding. The lead was peeled off as the bonding pressure P decreased. However, if P was higher than a certain value marked by the dotted lines in Fig. 7, the bump was broken or peeled off from the Al pad on the Si substrate (IC chip). Therefore, only the experimental points in the left hand side of the dotted lines show the bond-strength of the TAB inner lead bonding. Also, as the bonding pressure increases, the lead and bump is largely deformed, resulting in a low pull strength. Therefore, there is a optimal bonding pressure and as can be seen in Fig. 7, it is around P = 400 MPa for solid state inner lead bonding.

In fact, the pull strength depends on the deformation ratio rather than the bonding pressure, as shown in Fig. 8. The maximum strength is observed at the deformation ratio of 10 %, although the maximum strength in the liquid phase bonding occurred at a slightly smaller deformation ratio of 7.5 %. Bonding with a pressure of approximate 400 MPa should be carried out with a bonding time less than 1.0 s. However, as P increases, it becomes more difficult to control the bonding process during such a short time, especially for gang bonding. So, it is usually carried out in t = 0.5 s to 1.0 s. In the numerical simulation performed in the present study, P = 392 MPa and t = 0 s to 1.0 s were adopted as a standard.

As mentioned above, the pull strength largely depends on the bonding condition. In general, the bondability in microjoining of electronic packaging does not only depend

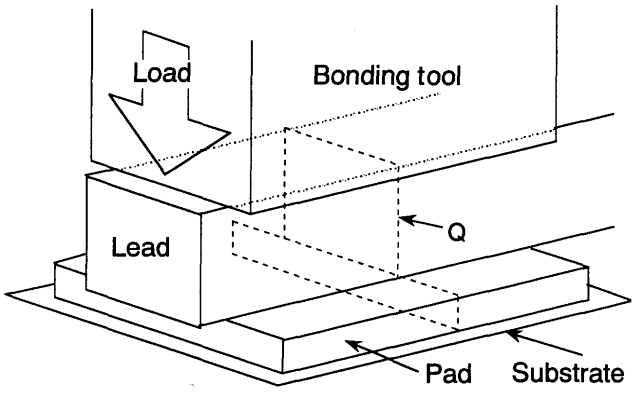

Fig. 9 Schematic illustration about simple model of inner lead bonding with flat tool.

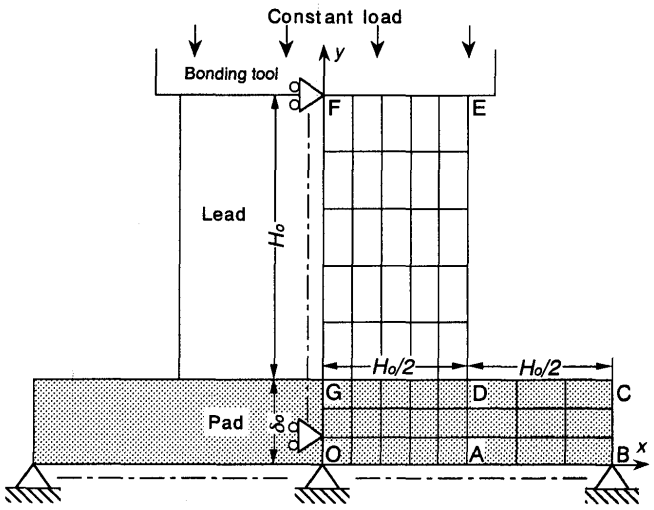

Fig. 10 Schematic illustration of initial mesh division on the cross section Q in Fig. 9.

on P and t but also the various parameters such as the bonding (specimen) temperature T, the bump (or pad) thickness δ_o , the pad mechanical properties and so on. It is, therefore, necessary to take into account these parameters in the numerical simulations.

4. Modeling of Inner Lead Bonding

Because the actual microjoining processes are complex, being affected by various parameters, it is very difficult to simulate it exactly. It is, thus, necessary to simplify it so that a specific parameter effect can be isolated, for example, the effect of bump thickness on the interfacial deformation can be discussed.

Fig. 9 shows a simple model of the inner lead bonding without ultrasonic vibration. Various bonding tools have been developed[8] but we treat only a flat tool in the present study. TAB leads are usually made of copper plated with

gold but it is assumed that both lead and pad are made of gold (same metal). It is also assumed that the substrate is too hard to deform and the cross section of the lead is a square. The lead height H_o is 10 μm. This value is equivalent to the minimum width of inner leads in TCP. The substrate is usually heated at 473-623 K and also the bonding tool is kept at about 773 K. Because of the heat input, temperature differs somewhat between lead and pad but the temperature of lead and pad is assumed to be constant at 573 K.

In our previous study[6], the deformation processes during wire thermocompression bonding were numerically analyzed and it was suggested that a fixed interface is more adequate than a slidable interface for predicting the bonding processes, i.e., once a wire contacts a pad, they are fixed to each other. In thermosonic bonding, local interface sliding must be produced by ultrasonic vibration at the beginning of bonding but the interface cannot slide after the adhesion is achieved. Therefore, in the present study, it is assumed that the interface between lead and pad (or bump) cannot slide during bonding.

The cross section Q in Fig. 9 is modeled by the finite element method which has been detailed elsewhere [4, 6]. The plane strain condition is assumed, where the deformation of lead and pad in the longitudinal direction of lead (the z direction) can be neglected. This is the valid when the bonding tool head is long enough in the z direction compared with the lead width, for example when the tool head is twice or more longer than the lead width. When the tool head length is close to the lead width, the strain rate in the z direction should be taken into account. However, even if the assumption of plane strain is adopted, the useful information will be obtained as stated below.

The initial mesh division in Q is shown in Fig. 10, where the z direction is perpendicular to the sheet. Because of symmetry, only the right hand side of the cross section Q was considered. The bonding load was assumed to be constant during bonding. In calculation, the displacement rate vectors $\dot{u}\,(\dot{u}_x,\dot{u}_y)$ on the tool interface FE were assigned so that the summation of the nodal forces applied on the FE could be finally equal to the constant load. In that stage, the x components $\dot{u}_x$ were all zero because of the tool constraint and the y components $\dot{u}_y$ were set to be equal to each other. The boundary condition on the FE satisfied the constant load and the tool constraint.

Fig. 11 schematically illustrates nodal points at the interface between lead and pad (or bump) in (a) and also de-

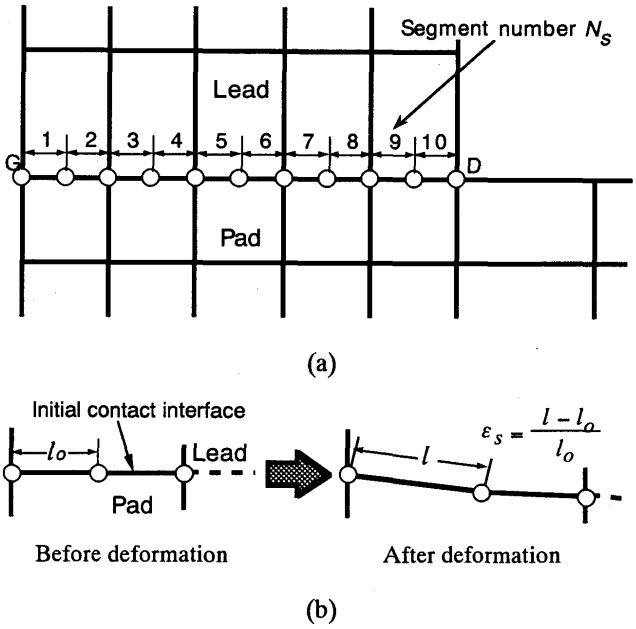

Fig. 11 Schematic illustration of bonding interface by FEM. (a) Nodal points and segment number at the bonding interface and (b) definitionof segment extension.

fines the interface-segment extension ε_s in (b). The calculation procedure has been detailed elsewhere [4, 5, 6, 9].

Both lead and pad (or bump) exhibit visco-plasticity and the strain rate $\dot{\bar{\varepsilon}}$ is given by

$$\dot{\bar{\varepsilon}} = A_0\left[1 + B\exp(-C\bar{\varepsilon})\right]\frac{D_0 bG}{kT}\left(\frac{\bar{\sigma}}{G}\right)^n \exp\left(-\frac{Q}{RT}\right), \tag{2}$$

where $\bar{\sigma}$ is the equivalent stress, $\bar{\varepsilon}$ is the equivalent strain, k is Boltzmann's constant, R is the gas constant, T is the bonding temperature in Kelvin and other constants are listed in Table 1.

The flow chart for computer simulation is shown in Fig. 12. One house code finite element model which the authors had developed was used for calculation [4]. It can treat very large deformation because it consists of eight-node isoparametric elements and Lagrange multipliers are taken into account. The converged solution was obtained by repeatedly solving the stiffness equation with respect to the perturbation $\Delta\{\dot{u}\}$ of the displacement rate vector $\{\dot{u}\}$, where the components of the perturbation $\Delta\{\dot{u}\}$ were assumed to be small deviations $\Delta\dot{u}$ from true values $\dot{u}$. The bonding load W_b is given by the bonding tool. The summation of the y direction nodal reaction forces at the interface between wire and tool (tool interface) is balanced by

Table 1 Material constants of gold lead.

Name	Symbol	Value	Unit
Frequency factor	D_o	0.1×10^{-4}	m^2s^{-1}
Constant	A_o	8.38×10^7	
Constant	B	1.5×10^2	
Constant	C	1.0×10^2	
Burgers vector	b	2.88×10^{-10}	m
Activation energy	Q	132.9	kJ mol^{-1}
Stress exponent	n	6.57	
Melting temperature	T_m	1336	K
Shear modulus	$G(T)$		Nm^{-2}

$$G(T) = a_G(T/T_m)^2 + b_G(T/T_m) + c_G$$

where $a_G = -9.9 \times 10^9$, $b_G = -6.2 \times 10^9$, $c_G = 3.1 \times 10^{10}$

the bonding load W_b but the individual reaction force value changes along the tool interface and is initially unknown. The y direction nodal forces at the tool interface cannot be given in advance as a boundary condition. Thus, a proper nodal displacement rate $\dot{u}$ with the same value was given to the nodal points at the tool interface and was fixed as the boundary conditions because it was known that the nodal points at the tool-interface can move with the same velocity in the y direction.

Fig. 13 is an illustration for explaining the relative difference in size between lead and bump. We here introduce the size ratio, δ_o/H_o, where δ_o is the initial thickness of bump as shown in Figs. 3 and 4. If we keep H_o constant and change only δ_o then an increase in the size ratio means the bump becomes thicker. On the other hand, if we fix δ_o and change only H_o, then the lead becomes smaller as the size ratio increases. A decrease in lead size is the same as an increase in bump thickness, if we consider the size effect in terms of δ_o / H_o. In other words, we can obtain the same interfacial deformation behavior due to thickening a bump (or pad), if we use finer TAB leads. Therefore, if we use δ_o / H_o then the size effect of lead and bump can be non dimensionalized.

In order to discuss the effect of pad mechanical properties on the interfacial extension, we introduce the parameter M, which is given by

$$M = A_{oP} / A_{oL} \quad \text{or} \quad A_{oB} / A_{oL}, \qquad (3)$$

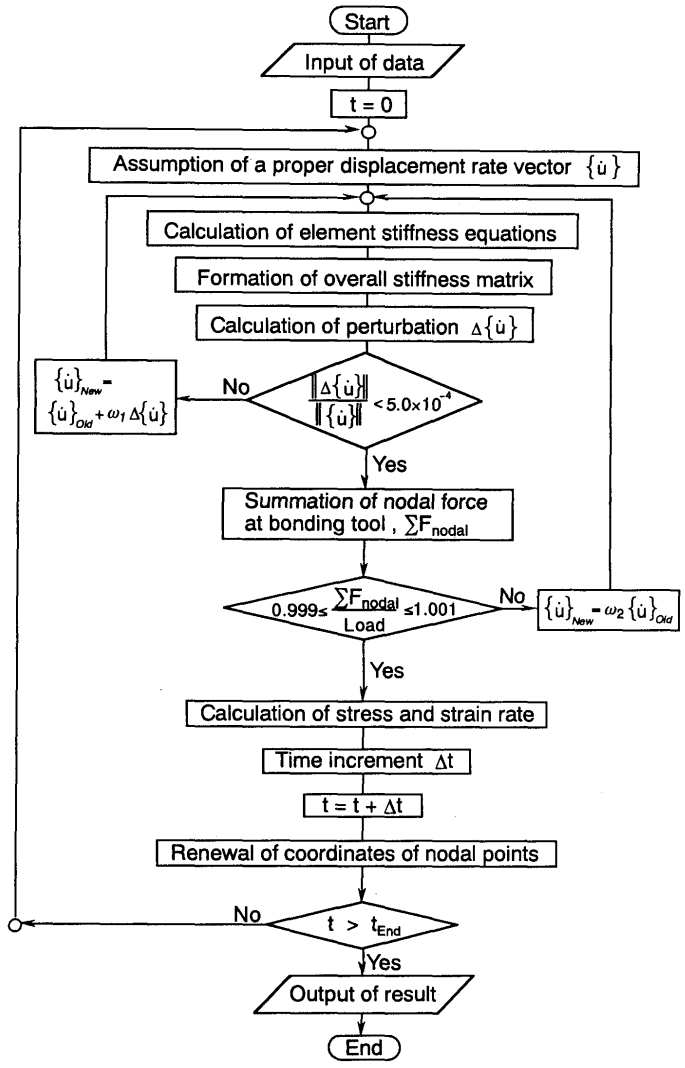

Fig. 12 Flow chart of computer simulation.

where the letters P, L and B in the subscripts mean pad, lead, and bump, respectively. A_{oP} is, therefore, A_o of pad. The strain rate in Eq. 2 largely depends on many material constants. Taking into account all of them will be a difficult job. Thus, in the present study, the influence of constant A_o on the strain rate was taken into consideration.

Table 2 shows the change in the values of the equivalent stress $\bar{\sigma}$ in pad (or bump) with M values. The $\bar{\sigma}$ in pad gives the same steady state strain rate produced by $\bar{\sigma}$ =100 MPa for the lead. If M = 1 then both $\bar{\sigma}$ are 100 MPa. As M increases, pad becomes soft and $\bar{\sigma}$ in pad decreases. M value increases approximately to 10^2 as the flow stress of pad falls to half. Further, we define the compression ratio $\Delta H/H_o$, where H_o is the initial lead height (width) and ΔH is the reduction of H_o after deformation. The parameter $\Delta H/H_o$ is useful when the interface extension and the stress distribution are compared.

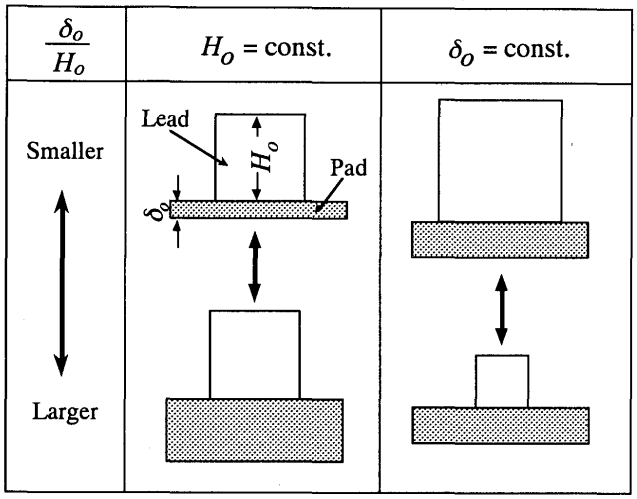

Fig. 13 Schematic illustration of relative size change between lead height H_o and pad thickness δ_o and definition of compression ratio (reduction) $\Delta H/H_o$.

Table 2 Equivalent stress value for pad or bump required to give the steady state strain rate attained for lead applied by 100 MPa.

M	$\bar{\sigma}$ for steady state (MPa)	
	Lead	Pad (or Bump)
10^6	100	12.2
10^4		24.6
10^2		49.6
1.0		100
10^{-2}		201.6

5. Numerical Results and Discussion

(1) Effect of Bump Thickness

Fig. 14 shows an example of the deformation process of lead and bump for δ_o/H_o = 0.5 (numerical result). The numbers at the top of each figure represent the absolute values of the displacement rate vector at the interface between tool and lead. As seen in Fig. 14, the bump is gradually indented by the lead with time and the lead exhibits the bulge-deformation. The bump-indentation becomes striking as δ_o/H_o increases but the bulge-deformation of the lead is evident as M decreases.

Fig. 15 shows the segment (interface) extension along the bond interface between lead and bump (or pad). The interface extension is largely affected by the parameter δ_o

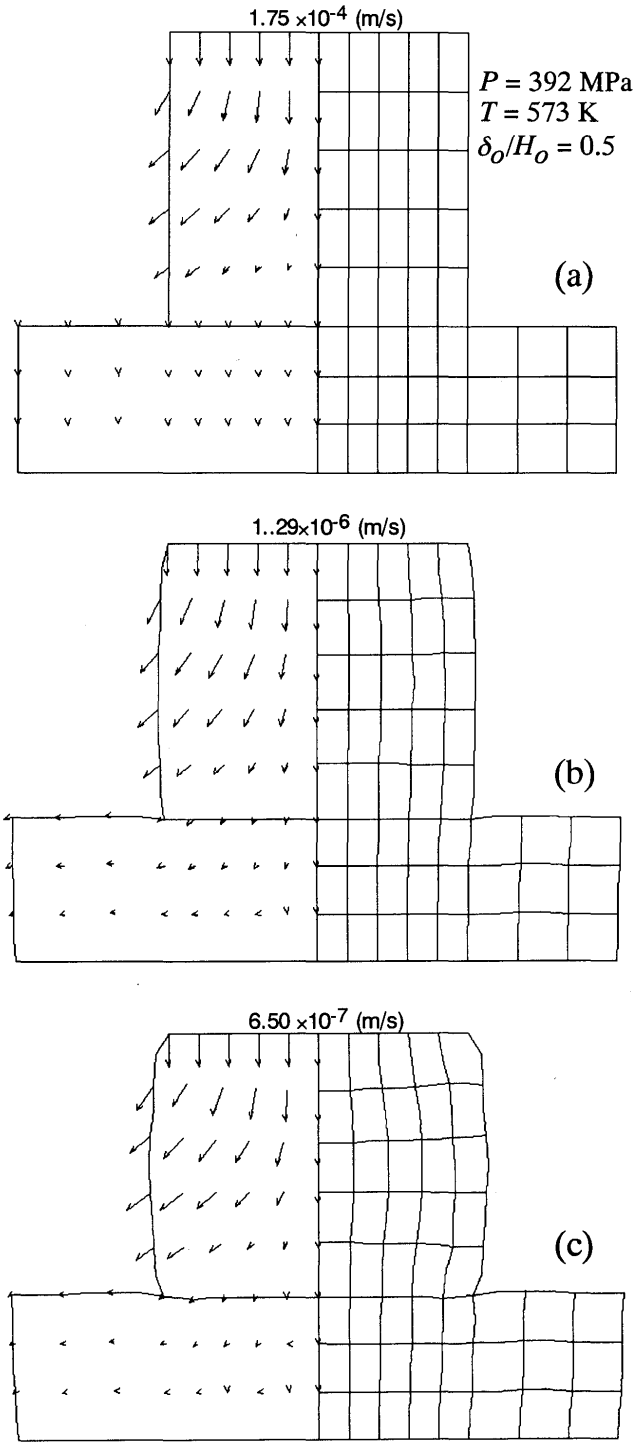

Fig. 14 Calculated results of deformation processes during TAB inner lead bonding.(M = 1).
(a) $\Delta H/H_o$ = 0.00%, t = 1.00x10^{-20}s,
(b) $\Delta H/H_o$ = 4.96%, t = 1.33x10^{-1}s,
(c) $\Delta H/H_o$ = 9.95 %, t = 7.38x10^{-1}s.

$/H_o$. The segment extension exhibits the maximum value at N_s = 8, but as δ_o/H_o increases, the extension becomes large at the center area, N_s = 1 to 4 of the bonded interface as seen in Fig. 15 (a). This means that the increase in δ_o facilitates the interfacial extension. In other words, the addition of the Au bump onto the electronic pad of the Si chip

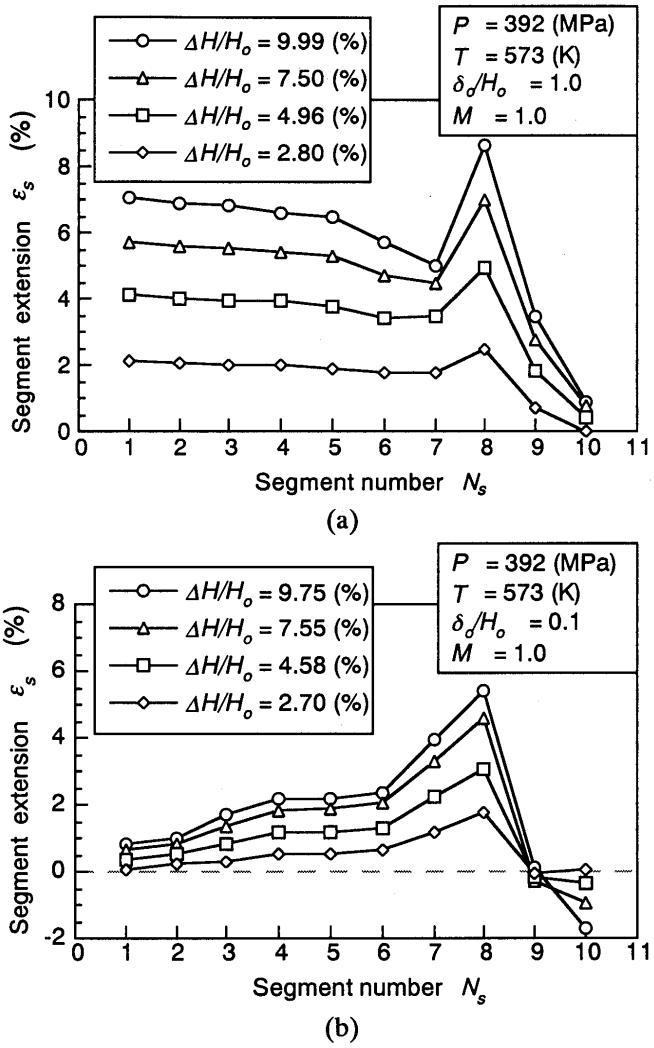

Fig. 15 Distribution of segment extension along bond-interface. (a) δ_o/H_o = 1.0, and (b) δ_o/H_o = 0.1.

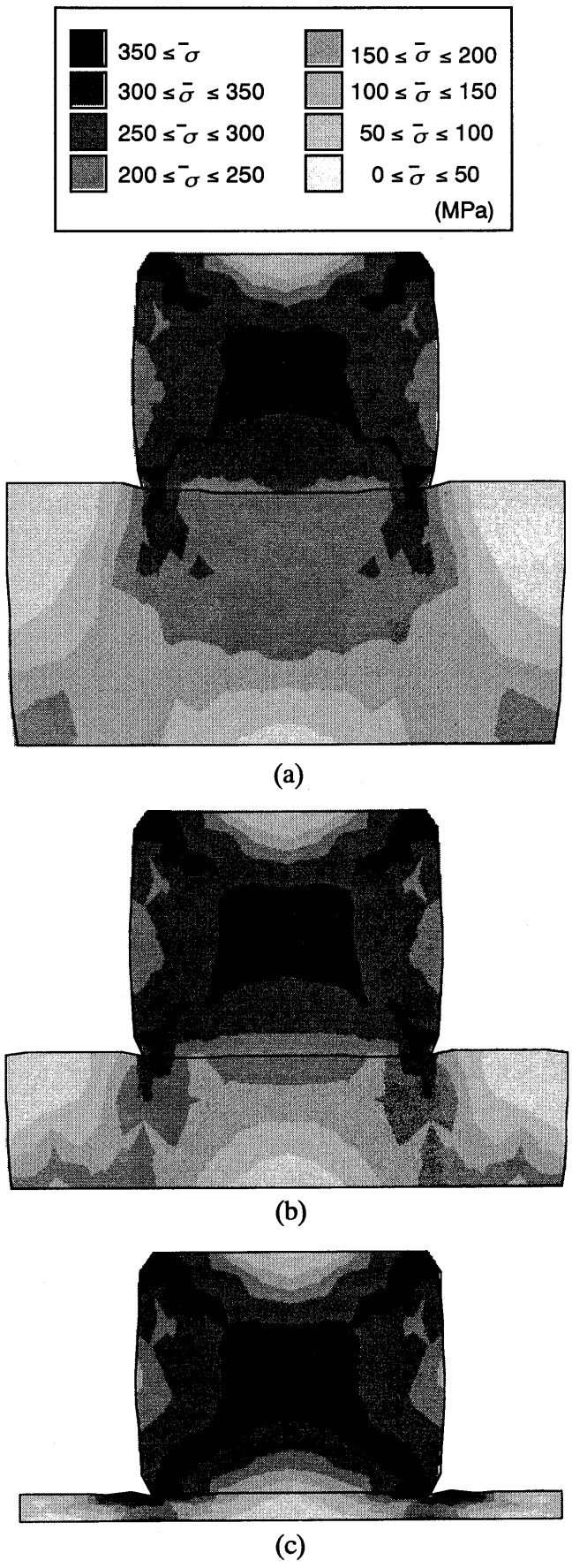

Fig. 16 Distribution of equivalent stress, depending on δ_o/H_o. (a) δ_o/H_o = 1.0, (b) δ_o/H_o = 0.5 and (c) δ_o/H_o = 0.1.

makes it easy to produce the interconnection between the Si chip and the TAB lead. It is, thus, guessed that the bumpless inner lead bonding introduced in Fig. 4 was very difficult [2], in which the ultrasonic vibration was introduced in order to decrease the flow stress for pad deformation by increasing the interface temperature (or soft Al pad must be used).

Fig. 16 shows the distribution of the equivalent stress depending on δ_o/H_o. The center of the lead exhibits high stress levels in all figures. Also, as δ_o/H_o increases, the stress concentration at the corner junction of the lead contacting the pad is reduced and the stress on the center area (N_s =1 to 6) of the interface between pad and lead relatively becomes high and uniform. As a result, the increase of δ_o/H_o facilitates the interfacial extension at the center area. Further, it is found that the stress distribution on the substrate is influenced by the thickness δ_o, i.e., the flow of

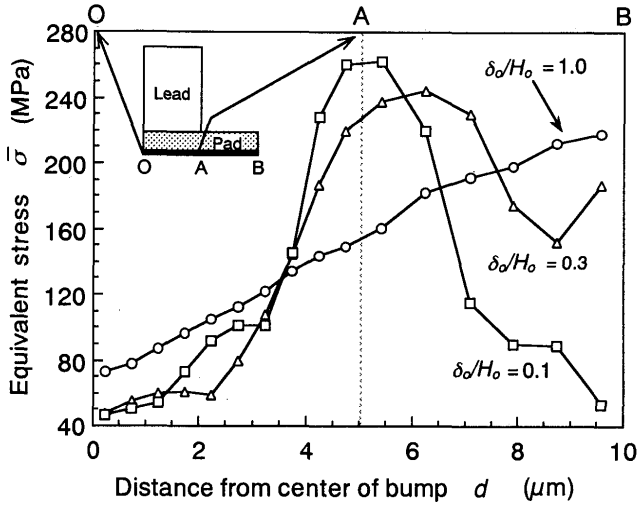

Fig. 17 Distribution of equivalent stress to the substrate.

stress from lead to the substrate can be improved by the bump. In other words, if a thick bump is used then the stress concentration produced at the lead edge can be dispersed by the bump and absorbed into the substrate. On the other hand, in the bumpless pad, the stress concentration cannot be dispersed through the pad and is directly applied to the substrate. Fig. 17 shows the stress distribution along the interface between the bump and the substrate.

(2) Effect of mechanical properties of pad

Bumpless bonding is largely influenced by the mechanical property of the pad (or lead frame for outer lead bonding). Thus, in the present study, the effect of pad mechanical properties on the interfacial extension between lead and pad is discussed, based on the numerical results simulated under the condition of δ_o/H_o = 0.1 (H_o =10 μm, δ_o = 1.0 μm).

Fig. 18 shows the effect of M values on the deformation pattern of lead and pad. A large value of M is means a soft pad material. $\Delta H/H_o$ is kept roughly at 10%. As M increases, the bond interface becomes to be expanded easily and the pad is largely deformed and heaped up (swollen) at both sides of the lead. On the other hand, the bulge-deformation of the lead is more striking at $M = 10^{-2}$.

Fig. 19 shows the segment extension along the bond interface between lead and pad. As M increases, the interfacial extension becomes large and exhibits the maximum value near the edge of the lead (N_s = 8). The compressive behaviors (minus extension) are observed at the edge of the lead. This is due to the constraint of the hard substrate and the swelling of pad material at both side of the lead.

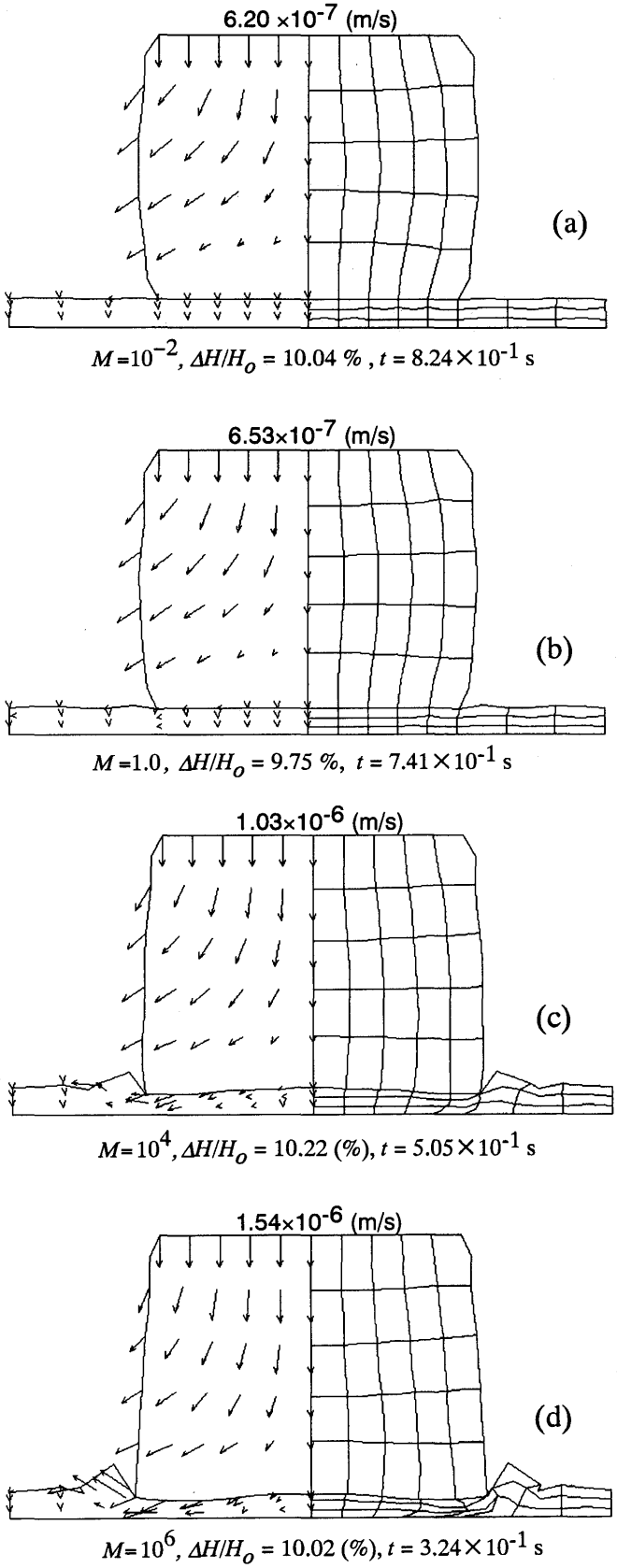

Fig. 18 Comparison of deformation patterns with change in M value.

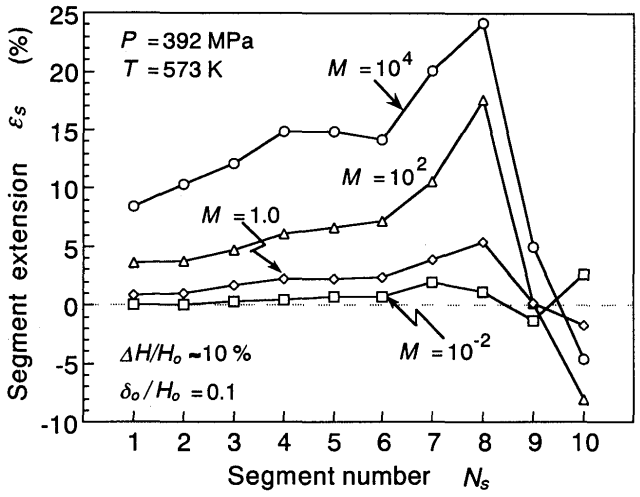

Fig. 19 Distribution of segment extension along bond interface, depending on M value.

Fig. 20 shows the equivalent stress distribution affected by M values. $\Delta H/H_o$ is approximately kept at 10 %. There is one point which is largely different from Fig. 16. It is the change in the stress distribution within the lead. As M increases, the stress becomes higher at the bottom of lead and this change facilitates the interface extension. Also, M value which is much greater than unity means that the pad is soft and the flow stress required for the pad deformation becomes low. Therefore, the pad can be easily extended.

However, the pad is also softened by raising the substrate temperature or decreasing the shear modulus G. Therefore, the parameter M should be redefined by

$$M = \frac{A_{oP} \cdot g_P}{A_{oL} \cdot g_L} \approx \frac{A_{oP} \cdot f_P}{A_{oL} \cdot f_L}, \qquad (4)$$

where the subscripts P and L denote pad and lead, respectively, g is expressed by

$$g = (G^{1-n} / T) \cdot \exp(-Q / RT), \qquad (5)$$

and also f is given by

$$f = \exp(-Q / RT). \qquad (6)$$

Equation (4) implies that M can be increased by selectively increasing the pad temperature. For example, if the substrate (or pad) temperature is be higher than that of the lead temperature, then large interfacial extension can be produced and the deformation damage of the lead becomes

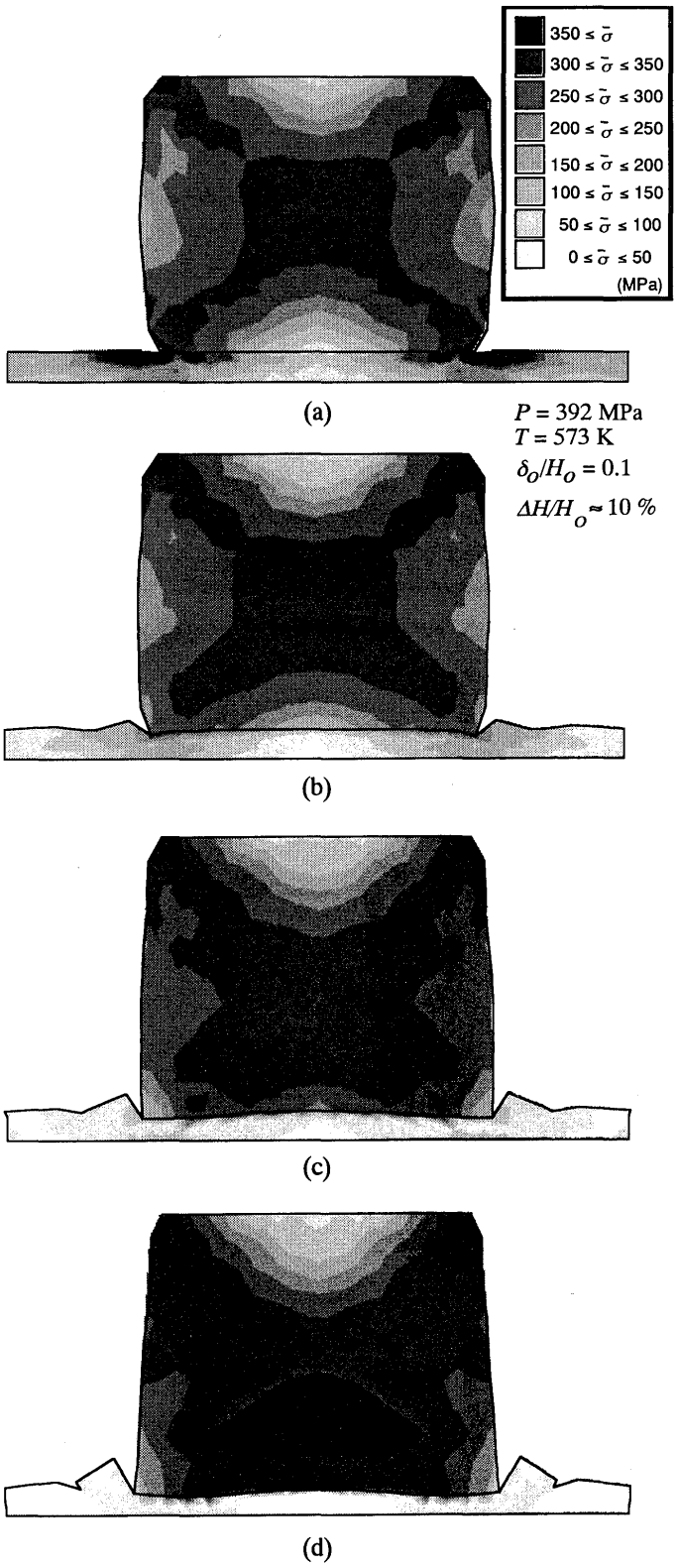

Fig. 20 Distribution of equivalent stress, depending on M value.
(a) $M = 10^{-2}$, (b) $M = 10^{2}$,
(c) $M = 10^{4}$, (d) $M = 10^{6}$.

smaller [10]. The increase in the substrate temperature makes it easy to produce the bumpless bonding. Or, the ultrasonic vibration can be applied into the interface as a friction energy at the beginning of bonding to increase the temperature at the bonding interface. As a result, preferential extension is produced at the interface and the good adhesion is attained[2]. It is not necessary to soften the pad itself as a material. As stated above, solid state microjoining is largely influenced by various factors but we are able to obtain a bond-strength much greater than that of the liquid phase microjoining as shown in Figs. 7 and 8.

6. Concluding Remarks

In this paper, the representative microjoining process used in electronic packaging were firstly introduced and their characteristics were summarized. The numerical simulation of TAB inner lead bonding was carried out and the deformation process during bonding was discussed, based on the calculated results. As mentioned above, the bonding process largely depends on various governing factors such as the bonding pressure, temperature, pad or bump thickness, and pad mechanical properties. The numerical simulation carried out in the present study will be helpful to optimize these factors. The main results obtained are as follows:

1) The bond-strength of solid state microjoining is much greater than that of liquid phase microjoining and can be obtained with the adequate bonding condition.

2) A TAB lead is often deformed like a bulge and the pad surface is swollen at the both sides of the lead edge in the actual TAB lead bonding. These phenomena are well simulated by the numerical model proposed in the present study.

3) As the size ratio of δ_o/H_o increases, the interfacial extension increases. When $\delta_o/H_o \leq 0.1$, the interface extension in the vicinity of the lead center is less than 2% in spite of the reduction $\Delta H/H_o$ = 10 %. On the other hand, when δ_o/H_o = 1.0, the interfacial extension is close to 8 % (see Fig. 14).

4) The pad thickness also influences the stress distribution. As the pad is thickened by the formation of the bump, the stress at the lead edge is dispersed into the bump and the damage to the substrate during bonding is reduced.

5) The stress distribution is largely influenced by the differences of temperature or mechanical property between lead and pad. As M decreases (temperature of pad is lower than that of lead), a stress concentration is produced under both sides of the lead edge. On the other hand, as M increases, the stress concentration is reduced.

6) A large M value produces a large interfacial extension. The maximum interfacial extension becomes much greater than the value of the compression ratio $\Delta H/H_o$. For example, a lead reduction of only $\Delta H/H_o$ =10% produces the maximum interfacial extension of 25% for M = 10^4 (see Fig. 19).

Acknowledgment

The present overview and numerical calculations were supported by Visiting Scholar Foundation of Key Laboratory in University of China.

References

1) T. Yamashita, Y. Iguchi, T. Kanamori, Y. Aramori, K. Ohno, and Y. Ohzaki, in Proc. Symp. High Density Packag. Technol. Applying High Pin Count Narrow Pitch Bonding, Japan Weld. Soc. Tokyo, Aug. 26th, (1992) pp. 41-49.

2) Y. Kurita, C. Kakegawa, and M. Urushima, in Proc. 4th Symp. Microjoining Assembly Technol. Electron. (MATE), Yokohama, Japan, Jan. 29-30, (1998) pp. 53-56.

3) N. Imaizumi, H. Tokuhira, M. Sasaki, H. Date, and E. Horikoshi, Proc. 5th Symp. Microjoining Assembly Technol. Electron.(MATE), Yokohama, Japan, Feb. 4 -5, (1999) pp. 163-168.

4) Y. Takahashi, T. Koguchi, and K. Nishiguchi, Trans. ASME J. Eng. Mater. Technol., Vol. 115, (1993) pp. 150-155.

5) Y. Takahashi and M. Tanimoto, Trans. ASME J. Eng. Mater. Technol., Vol. 117, (1995) pp. 330-335.

6) Y. Takahashi, S. Shibamoto and K. Inoue, IEEE Trans. CPMT, Part A, Vol. 19, (1996) pp. 213-223.

7) N. Bay, Metal Construction, Vol. 18, (1986) pp. 369-371.

8) T. Ando, T. Tomioka, M. Nakazono, K. Atsumi, Y. Tane, J. Nakano, and S. Hirata, IEEE Trans. CHMT, Vol. 16, No. 8, (1993) pp. 808-816.

9) Y. Takahashi, M. Inoue, and K. Inoue, IEEE Trans. CPT, Vol. 22, No. 2,(1999) pp. 291-298.

10) Y. Takahashi, M. Inoue, and K. Inoue, IEEE Trans. CPT, Vol. 22, No. 4,(1999) pp. 558-566.